Secrecy Analysis of Control Information for UAV

Huabing Lu, *Member, IEEE,* Zhaoyuan Shi, *Member, IEEE,* Nan Zhao, *Senior Member, IEEE,* Arumugam Nallanathan, *Fellow, IEEE,* and Xianbin Wang, *Fellow, IEEE*

***Abstract*—In this correspondence, we investigate the average achievable secrecy rate (AASR) and average effective secrecy throughput (AEST) of the control link from the ground control station to the unmanned aerial vehicle (UAV), which requires ultra-reliable and low-latency communications. Both the UAV and eavesdropper are assumed to be randomly distributed within the restricted areas, and short packet transmission is adopted to guarantee the low latency. We consider both free space and 3-Dimensional channel models for the UAV, and the statistic distribution functions of both models are given. By using Gaussian-Chebyshev quadrature (GCQ), the approximation expressions of AASR are derived to give insight on the design of packet size. Moreover, analytical expressions of ASET are also developed to evaluate the effective secrecy performance. Numerical results corroborate the correctness of our derived results.**

***Index Terms*—UAV, finite blocklength, physical layer security, ultra-reliable and low-latency communication.**

I. Introduction

DUE to the benefits of flexible mobility, fast deployment and excellent channels, unmanned aerial vehicle (UAV) communications have gained tremendous research attentions from both academia and industria [1], [2]. Particularly, UAVs can act as aerial platform for base stations, relays, and users [3], [4]. However, most of the existing UAV communications are based on conventional long-packet data transmission. To realize real-time control of fast-moving UAVs without collision, the control information delivery from the ground control station (GCS) to UAVs requires ultra low-latency and high reliability, compared with the conventional UAV data transmission.

Generally, the UAV control information packet is always quite short. To meet the ultra low-latency requirement, short-packet coding should be applied to control information. Hence, the conventional data transmission with long-packet coding is no longer applicable, and the conventional Shannon capacity based on the law of large numbers could overestimate the performance. Fortunately, the achievable rate of short-packet transmission with given decoding error has been developed in [5], based on which Ren *et al.* determined the average achievable data rate of UAV control information delivery system in [6]. Wang *et al.* investigated the average packet error probability and effective throughput performance of this system in [7].

The control information delivery is vulnerable to wiretaps due to the broadcast nature of wireless channels, more robust signals and often boosted power level. Hence, Yan *et al.* [8] jointly optimized the transmit power and the placement strategy of UAV short-packet covert communications. Zhou *et al.* [9] jointly optimized the UAV's 3-Dimensional (3D) placement and transmit power for covert communications with the objective of maximizing the communication covertness. [8] and [9] employ the covert communications to prevent the communication behavior from been detected by others nodes, but in some cases it is desirable to protect the transmitted information against eavesdropping by physical layer security. Recently, based on the short-packet secrecy transmission theory [10], Wang *et al.* [11] maximized the average effective secrecy rate of UAV short-packet transmission by jointly optimizing the UAV's trajectory and transmit power.

In this correspondence, we analyze the secure control information performance for the UAV with short-packet transmission by taking both the free space (FS) and 3D channel models into consideration. Both the complicated 3D channel model and the complex expression of the secrecy rate in short-packet transmission make the performance analysis quite involved. The contributions of this correspondence are outlined as follows: 1) We analyze the secrecy performance of UAV short-packet control information transmission by considering random node locations, and derive the distribution function of UAV for the 3D channel model; 2) The average achievable secrecy rate (AASR) of the considered system is analyzed by applying Gaussian-Chebyshev quadrature (GCQ); 3) We also derive the average effective secrecy throughput (AEST) performance of UAV control information delivery for both FS and 3D models.

II. System Model

As shown in Fig. 1, we consider a control information transmission system where the GCS sends ultra-reliable and low-latency communication (URLLC) signal to a UAV. Meanwhile, an eavesdropper tries to wiretap the confidential control information, and all nodes are equipped with a single antenna. Without loss of generality, assume that the GCS is located at the center of two concentric hemispheres, and the UAV is randomly distributed between the inner and outer hemispheres. The outer hemisphere with radius $D_{\max}$ represents the control range of GCS, and the inner hemisphere with radius $D_{\min}$ is introduced to be larger than the height of buildings to avoid collision. The eavesdropper is randomly distributed in a ring

H. Lu and N. Zhao are with the Key Laboratory of Intelligent Control and Optimization for Industrial Equipment of Ministry of Education, Dalian University of Technology, Dalian 116024, China (e-mail: luhuabing@dlut.edu.cn; zhaonan@dlut.edu.cn).

Z. Shi is with the Key Laboratory of Intelligent Perception and Computing of Anhui Province, Anqing Normal University, Anqing 246011, China (e-mail: shizy@stu.cqupt.edu.cn).

A. Nallanathan is with the School of Electronic Engineering and Computer Science, Queen Mary University of London, London E1 4NS, U.K. (e-mail: a.nallanathan@qmul.ac.uk).

X. Wang is with the Department of Electrical and Computer Engineering, Western University, London ON N6A 5B9, Canada (e-mail: xianbin.wang@uwo.ca).

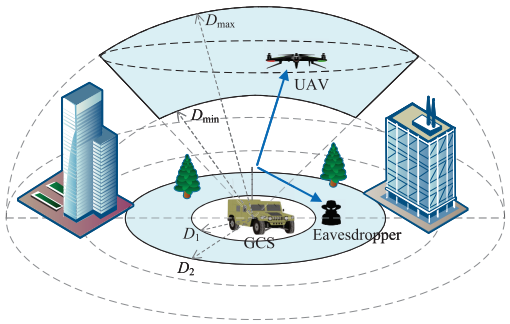

Fig. 1. Control information transmission with randomly distributed UAV and eavesdropper.

region also centered at the GCS with inner radius D_1 and outer radius D_2[1].

A. Eavesdropping Channel Model

Assume that the eavesdropping channel is invariant during each block and changes independently between blocks. Moreover, the channel is affected by both the large-scale path-loss and small-scale fading, modeled as $h_{\rm E} = g_{\rm E}(1+d_{\rm E}^{\alpha})^{-\frac{1}{2}}$ to avoid singular when $d_{\rm E}$ approaches 0 [12], where $d_{\rm E}$ denotes the distance from the GCS to the eavesdropper, α represents the path-loss exponent, and $g_{\rm E} \sim \mathcal{CN}(0,1)$ denotes Rayleigh fading. The transmit power of GCS is $P_{\rm G}$, and the noise power is denoted as σ^2. Hence, the received signal-to-noise ratio (SNR) at the eavesdropper can be denoted as $\gamma_{\rm E} = \frac{P_{\rm G}|g_{\rm E}|^2}{(1+d_{\rm E}^{\alpha})\sigma^2}$, whose cumulative distribution function (CDF) can be denoted as [12]

$$F_{\gamma_{\rm E}}(x) \approx (D_1+D_2)^{-1}\sum_{k=1}^{K}\Phi_k(1-e^{-c_k x}), \quad (1)$$

which is obtained by using GCQ [13], [14]. $c_k = (1+\phi_k^{\alpha})/\rho_{\rm G}$, $\Phi_k = \frac{\pi}{K}\sqrt{1-\varphi_k^2}\phi_k$, $\varphi_k = \cos(\frac{2k-1}{2K}\pi)$, $\phi_k = \frac{D_2+D_1}{2} + \frac{D_2-D_1}{2}\varphi_k$, K is the parameter to ensure the complexity-accuracy tradeoff, and $\rho_{\rm G} = P_{\rm G}/\sigma^2$ denotes the transmit SNR of GCS. By taking the first-order derivation of (1), we can obtain the probability density function (PDF) of $\gamma_{\rm E}$ as

$$f_{\gamma_{\rm E}}(x) \approx (D_1+D_2)^{-1}\sum_{k=1}^{K}\Phi_k c_k e^{-c_k x}. \quad (2)$$

B. UAV Channel Models

We consider two UAV channel models as follows.

1) FS Channel Model: The FS model is valid when the UAV is working in an obstacle-free area, such as the suburban areas. In this model, the line of sight (LoS) channel dominates the control link, and the channel gain is mainly decided by the link distance. Hence, the received SNR at UAV can be denoted as $\gamma_{\rm U}^{\rm FS} = \frac{\eta P_{\rm G}}{d_{\rm U}^2\sigma^2}$, where $d_{\rm U}$ represents the distance of the control link, and η is the channel power at a reference distance of 1 m. According to [7], the CDF of $\gamma_{\rm U}^{\rm FS}$ can be denoted as

$$F_{\gamma_{\rm U}^{\rm FS}}(x) = \begin{cases} 0, & x < \gamma_{\min}^{\rm FS} \\ \frac{D_{\max}^3 - (\eta\rho_{\rm G})^{\frac{3}{2}}x^{-\frac{3}{2}}}{\hat{D}_{\rm m}}, & \gamma_{\min}^{\rm FS} \le x \le \gamma_{\max}^{\rm FS} \\ 1, & x > \gamma_{\max}^{\rm FS} \end{cases} \quad (3)$$

[1]The proposed derivations can be also applied to the case of aerial eavesdroppers.

where $\gamma_{\min}^{\rm FS} = \frac{\eta\rho_{\rm G}}{D_{\max}^2}$, $\gamma_{\max}^{\rm FS} = \frac{\eta\rho_{\rm G}}{D_{\min}^2}$ and $\hat{D}_{\rm m} = D_{\max}^3 - D_{\min}^3$.

2) 3D Channel Model: In urban areas, the 3D channel model is more practical than FS. Both LoS and non-LoS (NLoS) channels are considered, and the probability of LoS increases with the elevation angle of UAV. Specifically, the LoS probability is [15]

$$P_{\rm LoS} = (1+a\exp(-b(\theta-a)))^{-1}, \quad (4)$$

where a and b are the environmental constants, θ is the elevation angle of UAV, the PDF of which can be denoted as $f_\theta(x) = 1/(\Theta_{\max}-\Theta_{\min})$, and $\Theta_{\max}$ and $\Theta_{\min}$ represent the maximal and maximum elevation angles of UAV, respectively. Accordingly, the NLoS probability is $P_{\rm NLoS} = 1 - P_{\rm LoS}$.

Accordingly, the path-loss models for both LoS and NLoS links in dB can be expressed as [15]

$$L_i = 20\log_{10}(4\pi f_c d c^{-1}) + \zeta_i, i \in \{\rm LoS, NLoS\}, \quad (5)$$

where f_c and c denote the carrier frequency and the speed of the light, respectively. Hence, the mean path-loss by considering the probability of both LoS and NLoS can be denoted as $L(\theta, d_{\rm U}) = P_{\rm LoS}L_{\rm LoS} + P_{\rm NLoS}L_{\rm NLoS}$. Combining (4) and (5), the path-loss can be denoted as

$$L(\theta, d_{\rm U}) = \frac{A_0}{1+a\exp(-b(\theta-a))} + 20\log_{10}(d_{\rm U}) + C_0, \quad (6)$$

where $A_0 = \zeta_{\rm LoS} - \zeta_{\rm NLoS}$, $C_0 = 20\log_{10}(4\pi f_c c^{-1}) + \zeta_{\rm NLoS}$.

Finally, the received SNR at UAV can be denoted as [7]

$$\gamma_{\rm U}^{\rm 3D} = \tilde{C}_0 d_{\rm U}^{-2}\exp[\tilde{A}_0/(1+a\exp(-b(\theta-a)))] = \tilde{d}\tilde{\theta}, \quad (7)$$

where $\tilde{A}_0 = -10^{-1}A_0\ln 10$, $\tilde{C}_0 = \rho_{\rm G}10^{-10^{-1}C_0}$, $\tilde{d} = \tilde{C}_0 d_{\rm U}^{-2}$ and $\tilde{\theta} = \exp[\tilde{A}_0/(1+a\exp(-b(\theta-a)))]$. The CDF of $\gamma_{\rm U}^{\rm 3D}$ is given in the following lemma.

Lemma 1: The CDF of UAV's SNR in the 3D model can be denoted as

$$F_{\gamma_{\rm U}^{\rm 3D}}(z) = \begin{cases} 0, & z < \tilde{\theta}_{\min}\tilde{d}_{\min} \\ F_{\gamma_{\rm U}^{\rm 3D}}^{\rm I}(z), & \tilde{\theta}_{\min}\tilde{d}_{\min} \le z \le \tilde{\theta}_{\max}\tilde{d}_{\min} \\ F_{\gamma_{\rm U}^{\rm 3D}}^{\rm II}(z), & \tilde{\theta}_{\max}\tilde{d}_{\min} < z < \tilde{\theta}_{\min}\tilde{d}_{\max} \\ F_{\gamma_{\rm U}^{\rm 3D}}^{\rm III}(z), & \tilde{\theta}_{\min}\tilde{d}_{\max} \le z \le \tilde{\theta}_{\max}\tilde{d}_{\max} \\ 1, & z > \tilde{\theta}_{\max}\tilde{d}_{\max} \end{cases} \quad (8)$$

where $\tilde{d}_{\min} = \frac{\tilde{C}_0}{D_{\max}^2}$, $\tilde{\theta}_{\min} = \exp(\frac{\tilde{A}_0}{a\exp(-b(\Theta_{\min}-a))+1})$, $\tilde{d}_{\max} = \frac{\tilde{C}_0}{D_{\min}^2}$ and $\tilde{\theta}_{\max} = \exp(\frac{\tilde{A}_0}{a\exp(-b(\Theta_{\max}-a))+1})$. $F_{\gamma_{\rm U}^{\rm 3D}}^{\rm I}(z)$, $F_{\gamma_{\rm U}^{\rm 3D}}^{\rm II}(z)$ and $F_{\gamma_{\rm U}^{\rm 3D}}^{\rm III}(z)$ are respectively shown in (34), (35) and (36), where $p_1(x) = \ln(\ln x) - \ln(\ln x - \tilde{A}_0)$ and $p_2(x) = {\rm Ei}(\frac{3}{2}\ln x) - \exp(\frac{3}{2}\tilde{A}_0){\rm Ei}(\frac{3}{2}(\ln x - \tilde{A}_0))$. Ei represents the exponential integral function [16, Eq. (8.211)], which is defined as ${\rm Ei}(z) = -\int_{-z}^{\infty} e^{-t}/t dt$.

Proof: Refer to the Appendix. ■

III. Analysis of AASR Performance

As the eavesdropping channel is unavailable, and both the locations of UAV and eavesdropper are uncertain, we cannot derive the exact secrecy performance of control information. Hence, we focus on the ergodic achievable secrecy performance by averaging the locations and eavesdropper's fading.

We first derive the AASR of control information to give insight on the design of packet size, which is defined as the average number of information bits that can be transmitted per channel use under given reliability and information leakage constraints. In finite-blocklength transmission, the lower bound of the achievable secrecy rate can be denoted as [10]

$$R_s = C_s - \sqrt{\frac{V_{\mathrm{U}}(\gamma_{\mathrm{U}})}{N}}\frac{Q^{-1}(\varepsilon)}{\ln 2} - \sqrt{\frac{V_{\mathrm{E}}(\gamma_{\mathrm{E}})}{N}}\frac{Q^{-1}(\delta)}{\ln 2} \quad (9)$$

in the case of $\gamma_{\mathrm{U}} > \gamma_{\mathrm{E}}$, otherwise $R_s = 0$. N denotes the blocklength, $C_s = \log_2(1+\gamma_{\mathrm{U}}) - \log_2(1+\gamma_{\mathrm{E}})$, $Q^{-1}(x)$ denotes the inverse of Gaussian Q-function with $Q(x) \triangleq \int_x^{+\infty}(\sqrt{2\pi})^{-1}\exp(-t^2/2)dt$, $V_j(\gamma_j) = 1-(1+\gamma_j)^{-2}$ with $j \in \{\mathrm{U},\mathrm{E}\}$ denotes the channel dispersion, ϵ denotes the decoding error probability constraint at UAV, and δ represents the secrecy constraint of information leakage. Based on (9), the lower bound of AASR can be denoted as [17]

$$\begin{aligned}\mathbb{E}[R_s] &= \mathbb{E}_{\gamma_{\mathrm{U}}}[\log_2(1+\gamma_{\mathrm{U}})] - \frac{Q^{-1}(\varepsilon)}{\sqrt{N}\ln 2}\mathbb{E}_{\gamma_{\mathrm{U}}}[\sqrt{V_{\mathrm{U}}(\gamma_{\mathrm{U}})}] \\ &\quad - \mathbb{E}_{\gamma_{\mathrm{E}}}[\log_2(1+\gamma_{\mathrm{E}})] - \frac{Q^{-1}(\delta)}{\sqrt{N}\ln 2}\mathbb{E}_{\gamma_{\mathrm{E}}}[\sqrt{V_{\mathrm{E}}(\gamma_{\mathrm{E}})}] \\ &\triangleq \Xi_{\gamma_{\mathrm{U}}} - \Xi_{\gamma_{\mathrm{U}},\varepsilon} - \Xi_{\gamma_{\mathrm{E}}} - \Xi_{\gamma_{\mathrm{E}},\delta}.\end{aligned} \quad (10)$$

For the third term of (10) $\Xi_{\gamma_{\mathrm{E}}}$, we have

$$\begin{aligned}\Xi_{\gamma_{\mathrm{E}}} &= \int_0^{\infty}\log_2(1+x)f_{\gamma_{\mathrm{E}}}(x)dx \\ &= \frac{1}{\ln 2}\int_0^{\infty}\frac{1}{1+x}(1-F_{\gamma_{\mathrm{E}}}(x))dx \\ &\overset{(a)}{=} \frac{1}{(D_2+D_1)\ln 2}\sum\nolimits_{k=1}^{K}\Phi_k\int_0^{\infty}\frac{e^{-c_n x}}{1+x}dx \\ &\overset{(b)}{=} \frac{-1}{(D_2+D_1)\ln 2}\sum\nolimits_{k=1}^{K}\Phi_k e^{c_k}\,\mathrm{Ei}(-c_k),\end{aligned} \quad (11)$$

where (a) can be obtained by using (1) and depends on $\sum_{k=1}^{K}\frac{\Phi_k}{D_1+D_2} = 1$, and (b) follows by applying [16, Eq. (3.352.4)]. The fourth term of (10) can be derived as

$$\begin{aligned}\Xi_{\gamma_{\mathrm{E}},\delta} &= \frac{Q^{-1}(\delta)}{\sqrt{N}\ln 2}\int_0^{\infty}\sqrt{1-(1+x)^{-2}}f_{\gamma_{\mathrm{E}}}(x)dx \\ &= \frac{Q^{-1}(\delta)}{\sqrt{N}\ln 2}\int_0^{\frac{\pi}{2}}\sqrt{1-(1+\tan y)^{-2}}f_{\gamma_{\mathrm{E}}}(\tan y)\sec^2 y dy \\ &\overset{(a)}{\approx} \frac{\pi^2 Q^{-1}(\delta)}{4K\sqrt{N}\ln 2}\sum\nolimits_{k=1}^{K}\sqrt{(1-\psi_k^2)(\tan^2\theta_k + 2\tan\theta_k)} \\ &\quad \times f_{\gamma_{\mathrm{E}}}(\tan\theta_k)\sec^2\theta_k/(1+\tan\theta_k),\end{aligned} \quad (12)$$

where (a) follows by using GCQ and $\theta_k = \frac{\pi}{4}(1+\psi_k)$, and $f_{\gamma_{\mathrm{E}}}(x)$ is shown in (2).

A. FS Channel Model

In the FS model, $\Xi_{\gamma_{\mathrm{U}}^{\mathrm{FS}}}$ can be derived as

$$\begin{aligned}\Xi_{\gamma_{\mathrm{U}}^{\mathrm{FS}}} &= \int_{\gamma_{\min}^{\mathrm{FS}}}^{\gamma_{\max}^{\mathrm{FS}}}\log_2(1+x)f_{\gamma_{\mathrm{U}}^{\mathrm{FS}}}(x)dx \\ &\overset{(a)}{=} \log_2(1+\gamma_{\min}^{\mathrm{FS}}) + \int_{\gamma_{\min}^{\mathrm{FS}}}^{\gamma_{\max}^{\mathrm{FS}}}\frac{1-F_{\gamma_{\mathrm{U}}^{\mathrm{FS}}}(x)}{1+x}dx \\ &\overset{(b)}{=} \log_2(1+\gamma_{\min}^{\mathrm{FS}}) + \frac{p_3(D_{\max}) - p_3(D_{\min})}{\hat{D}_{\mathrm{m}}\ln 2},\end{aligned} \quad (13)$$

where (a) is obtained by applying the integration-by-parts method, and (b) follows by substituting (3) and applying [16, Eq. (3.194.1)]. $p_3(x) = \frac{2}{3}x^3\,{}_2F_1(1,\frac{3}{2};\frac{5}{2};-\frac{x^2}{\eta\rho_{\mathrm{G}}}) + D_{\min}^3\ln(1+\frac{\eta\rho_{\mathrm{G}}}{x^2})$, and ${}_2F_1(\cdot)$ denotes the Gauss hypergeometric function [16, Eq. (9.111)]. Moreover, $\Xi_{\gamma_{\mathrm{U}}^{\mathrm{FS}},\delta}$ can be derived as

$$\begin{aligned}\Xi_{\gamma_{\mathrm{U}}^{\mathrm{FS}},\delta} &= \int_{\gamma_{\min}^{\mathrm{FS}}}^{\gamma_{\max}^{\mathrm{FS}}}\frac{Q^{-1}(\delta)}{\ln 2}\sqrt{\frac{V_{\mathrm{E}}(x)}{N}}f_{\gamma_{\mathrm{E}}}(x)dx \\ &\overset{(a)}{\approx} \frac{a_1\pi Q^{-1}(\delta)}{K\sqrt{N}\ln 2}\sum\nolimits_{k=1}^{K}\sqrt{(1-\psi_k^2)V_{\mathrm{E}}(\xi_k)}f_{\gamma_{\mathrm{E}}}(\xi_k),\end{aligned} \quad (14)$$

where (a) is obtained by applying GCQ, $a_1 = (\gamma_{\max}^{\mathrm{FS}} - \gamma_{\min}^{\mathrm{FS}})/2$, $a_2 = (\gamma_{\max}^{\mathrm{FS}} + \gamma_{\min}^{\mathrm{FS}})/2$ and $\xi_k = a_1\psi_k + a_2$. Finally, we can obtain the AASR of FS model by substituting (11), (12), (13) and (14) into (10).

B. 3D Channel Model

Due to the complicated expression of the CDF of $\gamma_{\mathrm{U}}^{\mathrm{3D}}$, it is challenging to derive the closed-form expression for $\Xi_{\gamma_{\mathrm{U}}^{\mathrm{3D}}}$ and $\Xi_{\gamma_{\mathrm{U}}^{\mathrm{3D}},\varepsilon}$. Hence, as [6], we apply GCQ to get an approximation expression as

$$\begin{aligned}&\Xi_{\gamma_{\mathrm{U}}^{\mathrm{3D}}} + \Xi_{\gamma_{\mathrm{U}}^{\mathrm{3D}},\varepsilon} \\ &= \frac{3\hat{D}_{\mathrm{m}}^{-1}}{\Theta_{\max}-\Theta_{\min}}\int_{D_{\min}}^{D_{\max}}d_{\mathrm{U}}^2\int_{\Theta_{\min}}^{\Theta_{\max}}R(\theta,d_{\mathrm{U}})d\theta dd_{\mathrm{U}} \\ &\approx \frac{3\pi^2(KM\hat{D}_{\mathrm{m}})^{-1}}{4(D_{\max}-D_{\min})}\sum_{m=1}^{M}\sum_{k=1}^{K}\sqrt{(1-\psi_k^2)(1-d_m^2)}R(\vartheta_k,d_m)d_m^2,\end{aligned} \quad (15)$$

where $\vartheta_k = (\Theta_{\max}+\Theta_{\min})/2 + (\Theta_{\max}-\Theta_{\min})\psi_k/2$, $t_m = \cos(\frac{2m-1}{2M}\pi)$, $d_m = (D_{\max}+D_{\min})/2 + (D_{\max}-D_{\min})t_m/2$, and M is the parameter for the complexity-accuracy tradeoff. $R(\theta,d_{\mathrm{U}}) = \log_2(1+\gamma_{\mathrm{U}}^{\mathrm{3D}}) - \sqrt{\frac{V_{\mathrm{U}}(\gamma_{\mathrm{U}}^{\mathrm{3D}})}{N}}\frac{Q^{-1}(\varepsilon)}{\ln 2}$, and $\gamma_{\mathrm{U}}^{\mathrm{3D}}$ shown in (9) is a function of θ and d_{U}. By substituting (11), (12) and (15) into (10), we can obtain the AASR of 3D model.

IV. Analysis of AEST Performance

In this section, we analyze the AEST performance, which is defined as the average secrecy rate at which the data packet can be reliably transmitted under a certain secrecy constraint [18]. Assume that the GCS transmits L bits data in each short-packet transmission, and the transmission rate is $R = L/N$ for a given blocklength N. Substituting R into (9), the decoding error can be denoted as

$$\varepsilon = Q[\sqrt{\frac{N}{V_{\mathrm{U}}(\gamma_{\mathrm{U}})}}(\ln\frac{1+\gamma_{\mathrm{U}}}{1+\gamma_{\mathrm{E}}} - \sqrt{\frac{V_{\mathrm{E}}(\gamma_{\mathrm{E}})}{N}}Q^{-1}(\delta) - \frac{L\ln 2}{N})], \quad (16)$$

when $\gamma_{\mathrm{U}} > \gamma_{\mathrm{E}}$; otherwise, $\varepsilon = 1$. Hence, the AEST can be denoted as

$$T_{\mathrm{s}} = \mathbb{E}[(1-\varepsilon)L/N] = (1-\bar{\varepsilon})L/N, \quad (17)$$

where $\bar{\varepsilon} \triangleq \mathbb{E}_{\gamma_{\mathrm{U}},\gamma_{\mathrm{E}}}[\varepsilon]$, which is averaged over γ_{U} and γ_{E}. Hence, we have

$$T_{\mathrm{s}} = \frac{L}{N} - \frac{L}{N}\int_0^{\infty}\int_0^{\infty}\varepsilon f_{\gamma_{\mathrm{U}}}(x)dx f_{\gamma_{\mathrm{E}}}(y)dy. \quad (18)$$

Since ε in (16) is complex, we apply the first-order approximation to simplify it as [19]

$$\varepsilon(x) \approx \begin{cases} 1, & x < x_m \\ 2^{-1} - \varpi(x - x_0), & x_m \le x \le x_M \\ 0, & x > x_M \end{cases} \tag{19}$$

where $x_0 = \exp\{\sqrt{V_{\rm E}(\gamma_{\rm E})N^{-1}}Q^{-1}(\delta) + \frac{L}{N}\ln 2\}(1+\gamma_{\rm E}) - 1$, $\varpi = \sqrt{N(2\pi x_0(x_0+2))^{-1}}$, $x_m = x_0 - (2\varpi)^{-1}$, $x_M = x_0 + (2\varpi)^{-1}$. Then, we define

$$\begin{aligned} \Psi(\gamma_{\rm E}) &= \int_0^{\infty} \varepsilon_{\gamma_{\rm U}|\gamma_{\rm E}} f_{\gamma_{\rm U}}(x)dx \\ &= F_{\gamma_{\rm U}}(x_m) + \int_{x_m}^{x_M} (\frac{1}{2} - \varpi(x - x_0)) f_{\gamma_{\rm U}}(x)dx \\ &\overset{(a)}{=} \varpi \int_{x_m}^{x_M} F_{\gamma_{\rm U}}(x)dx, \end{aligned} \tag{20}$$

where (a) is obtained by using the integration-by-parts method. Since ϖ is large enough, by applying the Riemann integral approximation, (20) can be further denoted as

$$\Psi(\gamma_{\rm E}) = \varpi F_{\gamma_{\rm U}}(x_0)(x_M - x_m) = F_{\gamma_{\rm U}}(x_0). \tag{21}$$

Substituting (21) into (18), we have

$$T_{\rm s} = \frac{L}{N} - \frac{L}{N}\int_0^{\infty} F_{\gamma_{\rm U}}(x_0) f_{\gamma_{\rm E}}(y)dy. \tag{22}$$

Since the CDFs of UAV's SNRs for both FS and 3D models are piecewise functions, we apply the change-in-variable technique to make further derivation. With the increasing of $\gamma_{\rm E}$, $V_{\rm E}(\gamma_{\rm E}) = 1 - (1+\gamma_{\rm E})^{-2}$ can be approximated as 1 without losing much accuracy [20], and we have $x_0 \approx \exp\{\frac{1}{\sqrt{N}}Q^{-1}(\delta) + \frac{L}{N}\ln 2\}(1+y) - 1 = \beta(1+y) - 1$, where $\beta = \exp\{\frac{1}{\sqrt{N}}Q^{-1}(\delta) + \frac{L}{N}\ln 2\}$. Substituting $y = \frac{x_0}{\beta} + \frac{1-\beta}{\beta}$ into (22), we have

$$T_{\rm s} = \frac{L}{N} - \frac{L}{N\beta}\int_{\beta-1}^{\infty} F_{\gamma_{\rm U}}(x_0) f_{\gamma_{\rm E}}(\frac{x_0}{\beta} + \frac{1-\beta}{\beta})dx_0. \tag{23}$$

A. FS Channel Model

Define $\lambda_{\min} \triangleq \max(\beta - 1, \gamma_{\min}^{\rm FS})$ and $\lambda_{\max} \triangleq \max(\beta - 1, \gamma_{\max}^{\rm FS})$. According to (23) and (3), the AEST for the FS model can be denoted as

$$\begin{aligned} T_{\rm s}^{\rm FS} &= \frac{L}{N} - \frac{L}{N\beta}\int_{\lambda_{\min}}^{\infty} F_{\gamma_{\rm U}^{\rm FS}}(x_0) f_{\gamma_{\rm E}}(\frac{x_0}{\beta} + \frac{1-\beta}{\beta})dx_0 \\ &= \underbrace{\frac{L}{N} - \frac{L}{N\beta}\int_{\lambda_{\max}}^{\infty} f_{\gamma_{\rm E}}(\frac{x_0}{\beta} + \frac{1-\beta}{\beta})dx_0}_{T_{\rm s}^{\rm FS,I}} \\ &\quad \underbrace{- \frac{L}{N\beta}\int_{\lambda_{\min}}^{\lambda_{\max}} F_{\gamma_{\rm U}^{\rm FS}}(x_0) f_{\gamma_{\rm E}}(\frac{x_0}{\beta} + \frac{1-\beta}{\beta})dx_0}_{T_{\rm s}^{\rm FS,II}}. \end{aligned} \tag{24}$$

By applying (3), we have $T_{\rm s}^{\rm FS,I} = p_4(\lambda_{\max})$, where $p_4(x) = \frac{L}{N}F_{\gamma_{\rm E}}(\frac{x}{\beta} + \frac{1-\beta}{\beta})$.

Moreover, by using integration-by-parts and [16, Eq. (3.381.1)], $T_{\rm s}^{\rm FS,II}$ can be derived as

$$\begin{aligned} T_{\rm s}^{\rm FS,II} &= D_{\max}^3 \hat{D}_{\rm m}^{-1}[p_4(\lambda_{\max}) - p_4(\lambda_{\min})] \\ &+ \frac{2L(\rho_{\rm A}\eta)^{\frac{3}{2}}}{N\beta\hat{D}_{\rm m}}[p_5(\lambda_{\max}) - p_5(\lambda_{\min}) + \frac{\beta^{-\frac{1}{2}}}{D_2 + D_1}\sum_{k=1}^{K}\Phi_k \\ &\times c_k^{\frac{3}{2}} e^{-c_k\frac{1-\beta}{\beta}}(\gamma(\frac{1}{2}, \frac{c_k\lambda_{\max}}{\beta}) - \gamma(\frac{1}{2}, \frac{c_k\lambda_{\min}}{\beta}))], \end{aligned} \tag{25}$$

where $p_5(x) = f_{\gamma_{\rm E}}(\frac{x}{\beta} + \frac{1-\beta}{\beta})x^{-\frac{1}{2}}$. $\gamma(\alpha, x) = \int_0^x e^{-t}t^{\alpha-1}dt$ denotes the lower incomplete Gamma function. Finally, substituting the expressions of $T_{\rm s}^{\rm FS,I}$ and $T_{\rm s}^{\rm FS,II}$ into (24), we can obtain the AEST of the FS model.

B. 3D Channel Model

According to Lemma 1, we set $\Lambda_1 = \max\{\tilde{\theta}_{\min}\tilde{d}_{\min}, \beta-1\}$, $\Lambda_2 = \max\{\tilde{\theta}_{\max}\tilde{d}_{\min}, \beta-1\}$, $\Lambda_3 = \max\{\tilde{\theta}_{\min}\tilde{d}_{\max}, \beta-1\}$ and $\Lambda_4 = \max\{\tilde{\theta}_{\max}\tilde{d}_{\max}, \beta-1\}$. Based on (8), the average secrecy throughput in (23) can be converted to

$$\begin{aligned} T_{\rm s}^{\rm 3D} = &\underbrace{-\frac{L}{N\beta}\int_{\Lambda_1}^{\Lambda_2} F_{\gamma_{\rm U}^{\rm 3D}}^{\rm I}(x_0) f_{\gamma_{\rm E}}(\frac{x_0}{\beta} + \frac{1-\beta}{\beta})dx_0}_{T_{\rm s}^{\rm 3D,I}} \\ &\underbrace{-\frac{L}{N\beta}\int_{\Lambda_2}^{\Lambda_3} F_{\gamma_{\rm U}^{\rm 3D}}^{\rm II}(x_0) f_{\gamma_{\rm E}}(\frac{x_0}{\beta} + \frac{1-\beta}{\beta})dx_0}_{T_{\rm s}^{\rm 3D,II}} \\ &\underbrace{-\frac{L}{N\beta}\int_{\Lambda_3}^{\Lambda_4} F_{\gamma_{\rm U}^{\rm 3D}}^{\rm III}(x_0) f_{\gamma_{\rm E}}(\frac{x_0}{\beta} + \frac{1-\beta}{\beta})dx_0}_{T_{\rm s}^{\rm 3D,III}} \\ &\underbrace{+\frac{L}{N} - \frac{L}{N\beta}\int_{\Lambda_4}^{\infty} f_{\gamma_{\rm E}}(\frac{x_0}{\beta} + \frac{1-\beta}{\beta})dx_0}_{T_{\rm s}^{\rm 3D,IV}}. \end{aligned} \tag{26}$$

It is challenging to derive the closed-form expressions for $T_{\rm s}^{\rm I}$, $T_{\rm s}^{\rm II}$ and $T_{\rm s}^{\rm III}$, since both $F_{\gamma_{\rm U}^{\rm 3D}}$ and $f_{\gamma_{\rm E}}$ are quite involved. We apply GCQ to get an approximation expression as

$$\begin{aligned} &T_{\rm s}^{\rm 3D,I} + T_{\rm s}^{\rm 3D,II} + T_{\rm s}^{\rm 3D,III} \\ &= \frac{\pi L}{KN\beta}\sum_{k=1}^{K}\sqrt{1-\psi_k^2}[\hat{\Lambda}_1 F_{\gamma_{\rm U}^{\rm 3D}}^{\rm I}(s_k^{\rm I}) f_{\gamma_{\rm E}}(\frac{s_k^{\rm I}+1-\beta}{\beta}) \\ &+ \hat{\Lambda}_2 F_{\gamma_{\rm U}^{\rm 3D}}^{\rm II}(s_k^{\rm II}) f_{\gamma_{\rm E}}((s_k^{\rm II}+1-\beta)\beta^{-1}) \\ &+ \hat{\Lambda}_3 F_{\gamma_{\rm U}^{\rm 3D}}^{\rm III}(s_k^{\rm III}) f_{\gamma_{\rm E}}((s_k^{\rm III}+1-\beta)\beta^{-1})], \end{aligned} \tag{27}$$

where $s_k^{\rm I} = (\Lambda_2+\Lambda_1)/2 - \hat{\Lambda}_1\psi_k$, $s_k^{\rm II} = (\Lambda_3+\Lambda_2)/2 - \hat{\Lambda}_2\psi_k$, $s_k^{\rm III} = (\Lambda_4+\Lambda_3)/2 - \hat{\Lambda}_3\psi_k$, $\hat{\Lambda}_1 = (\Lambda_1-\Lambda_2)/2$, $\hat{\Lambda}_2 = (\Lambda_2-\Lambda_3)/2$ and $\hat{\Lambda}_3 = (\Lambda_3-\Lambda_4)/2$. $T_{\rm s}^{\rm 3D,IV}$ can be derived as

$$\begin{aligned} T_{\rm s}^{\rm IV} &= \frac{L}{N} - \frac{L}{N\beta}\int_{\Lambda_4}^{\infty} f_{\gamma_{\rm E}}((x_0+1-\beta)\beta^{-1})dx_0 \\ &= LN^{-1}F_{\gamma_{\rm E}}((\Lambda_4+1-\beta)\beta^{-1}). \end{aligned} \tag{28}$$

Finally, we can get the AEST of the 3D model by adding (27) and (28).

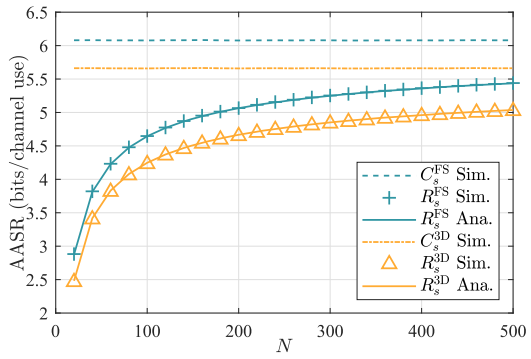

Fig. 2. AASR versus N for two channel models of UAV.

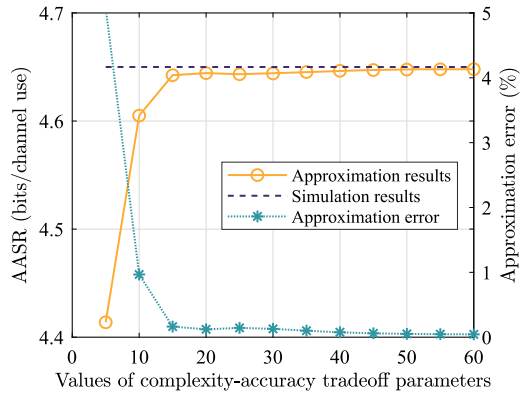

Fig. 3. Accuracy of applying GCQ.

V. Simulation Results and Discussion

Simulation results are provided to evaluate the above analysis. Hereinafter, unless specified, the simulation parameters are set according to [6], [21] as $D_{\min} = 100$ m, $D_{\max} = 300$ m, $D_1 = 300$ m, $D_2 = 800$ m, $\Theta_{\min} = 45$, $\Theta_{\max} = 90$, $P_G = -20$ dB, $L = 200$, $\varepsilon = 10^{-9}$, $\sigma^2 = -173$ dBm/Hz, $B = 10$ MHz, $f_c = 2$ GHz, $c = 3 \cdot 10^8$ m/s, $\alpha = 3.8$, $a = 12.08$, $b = 0.11$, $\zeta_{\text{LoS}} = 1.6$, $\zeta_{\text{NLoS}} = 23$ and $\eta = -40$ dB.

In Fig. 2, we study the AASR with N, where $\delta = 10^{-5}$. For comparison with the long-packet transmission, we also plot the conventional secrecy capacity of $C_s = \log_2(1+\gamma_U) - \log_2(1+\gamma_E)$. We can observe from Fig. 2 that the developed analytical expressions match well with simulation results. We can also see that when N is relatively small, there is a sharp gap between the conventional secrecy capacity and the AASR. However, the AASR is increasing with N and approaches the secrecy capacity gradually, because the second and third terms in (9) diminish with N. This observation shows that the performance will be overestimated when adopting the conventional secrecy capacity, and the short-packet secrecy transmission theory should be adopted to design the parameters for URLLC applications.

In Fig. 3, we apply simulation results to show the approximation accuracy for applying GCQ [13], [14], where $N = 100$ and $\delta = 10^{-5}$. The approximation results for FS model are obtained with (12) and (14), and the simulation results are acquired by averaging over 10^6 independent trials.

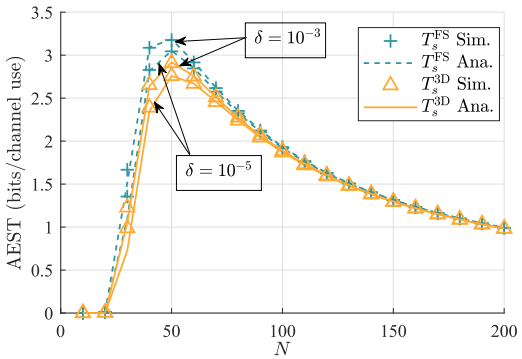

Fig. 4. AEST versus N for two channel models of UAV.

It can be observed from the figure that the approximation error decreases with the uplift of the values of complexity-accuracy trade-off parameters. It can also be observed that the approximation values is very close to the simulation results (approximation error less than 1%) when the complexity accuracy trade-off parameters are set as 20.

Fig. 4 plots the AEST with different information leakage constraint. It can be observed that the analytical expressions match well with simulation results, which verifies the correctness of our theoretical analysis. As anticipated, the AEST will be deteriorated with more stringent information leakage requirement, and the FS model can achieve better performance than the 3D model. Moreover, it can be observed that the AEST performance increases first and then decreases with N. This observation can be explained by (17), which indicates that the AEST is a multiplication of the successful decoding probability and transmission rate. When the blocklength N is small, the decoding error is quite high, and the transmission rate is quite low when N is large.

VI. Conclusion

In this correspondence, we investigated the AASR and AEST performance of a UAV control information delivery system with randomly deployed UAV and eavesdropper. Both FS and 3D channel models of UAV were considered under the short-packet transmission. The GCQ method was applied to derive the approximate expressions of AASR and AEST. These results provide insights for the packet size and blocklength design when the system should guarantee a target security and reliability performance.

Appendix

We only consider the case of $\tilde{\theta}_{\max}\tilde{d}_{\min} < \tilde{\theta}_{\min}\tilde{d}_{\max}$ for space limitation, and the case of $\tilde{\theta}_{\max}\tilde{d}_{\min} > \tilde{\theta}_{\min}\tilde{d}_{\max}$ can be derived similarly. First, the CDF of γ_U^{3D} can be denoted as

$$F_{\gamma_U^{3D}}(z) = P(\tilde{d}\tilde{\theta} < z) = P(\tilde{d} < z\tilde{\theta}^{-1}). \quad (29)$$

Based on the value of z, $F_{\gamma_{\mathrm{U}}^{\mathrm{3D}}}(z)$ can be divided into the following five cases:

$$F_{\gamma_{\mathrm{U}}^{\mathrm{3D}}}(z)=\begin{cases}0, & z<\tilde{\theta}_{\min}\tilde{d}_{\min}\\ F_{\gamma_{\mathrm{U}}^{\mathrm{3D}}}^{\mathrm{I}}(z)\triangleq\int_{\tilde{\theta}_{\min}}^{\frac{z}{\tilde{d}_{\min}}}\int_{\tilde{d}_{\min}}^{\frac{z}{y}}f_{\tilde{d},\tilde{\theta}}(x,y)dxdy, & \\ \qquad\tilde{\theta}_{\min}\tilde{d}_{\min}\le z\le\tilde{\theta}_{\max}\tilde{d}_{\min}\\ F_{\gamma_{\mathrm{U}}^{\mathrm{3D}}}^{\mathrm{II}}(z)\triangleq\int_{\tilde{\theta}_{\min}}^{\tilde{\theta}_{\max}}\int_{\tilde{d}_{\min}}^{\frac{z}{y}}f_{\tilde{d},\tilde{\theta}}(x,y)dxdy, & \\ \qquad\tilde{\theta}_{\max}\tilde{d}_{\min}<z<\tilde{\theta}_{\min}\tilde{d}_{\max}\\ F_{\gamma_{\mathrm{U}}^{\mathrm{3D}}}^{\mathrm{III}}(z)\triangleq 1-\int_{\frac{z}{\tilde{d}_{\max}}}^{\tilde{\theta}_{\max}}\int_{\frac{z}{y}}^{\tilde{d}_{\max}}f_{\tilde{d},\tilde{\theta}}(x,y)dxdy, & \\ \qquad\tilde{\theta}_{\min}\tilde{d}_{\max}\le z\le\tilde{\theta}_{\max}\tilde{d}_{\max}\\ 1. & z>\tilde{\theta}_{\max}\tilde{d}_{\max}\end{cases}\tag{30}$$

Since $\tilde{d}$ and $\tilde{\theta}$ are independent, we know $f_{\tilde{d},\tilde{\theta}}(x,y)=f_{\tilde{d}}(x)f_{\tilde{\theta}}(y)$. According to [7], when $\tilde{\theta}_{\min}<\tilde{\theta}<\tilde{\theta}_{\max}$, the PDF of $\tilde{\theta}$ can be denoted as

$$f_{\tilde{\theta}}(x)=\tilde{A}_0[b(\Theta_{\max}-\Theta_{\min})(\tilde{A}_0-\ln x)x\ln x]^{-1},\tag{31}$$

and the CDF of $\tilde{d}$ can be expressed as

$$F_{\tilde{d}}(x)=\begin{cases}0, & x<\tilde{d}_{\min}\\ \frac{D_{\max}^3-(\tilde{C}_0x^{-1})^{\frac{3}{2}}}{\hat{D}_{\mathrm{m}}}, & \tilde{d}_{\min}<x<\tilde{d}_{\max}\\ 1. & x>\tilde{d}_{\max}\end{cases}\tag{32}$$

Then, by applying (30), (31) and (32), we have

$$\begin{aligned}F_{\gamma_{\mathrm{U}}^{\mathrm{3D}}}^{\mathrm{I}}(z)&=\int_{\tilde{\theta}_{\min}}^{\frac{z}{\tilde{d}_{\min}}}f_{\tilde{\theta}}(y)[F_{\tilde{d}}(zy^{-1})-F_{\tilde{d}}(\tilde{d}_{\min})]dy\\&=\int_{\tilde{\theta}_{\min}}^{\frac{z}{\tilde{d}_{\min}}}\frac{\Delta_0\tilde{A}_0D_{\max}^3y^{-1}}{(\tilde{A}_0-\ln y)\ln y}dy\\&\quad-\int_{\tilde{\theta}_{\min}}^{\frac{z}{\tilde{d}_{\min}}}\frac{\Delta_0\tilde{A}_0(\tilde{C}_0)^{\frac{3}{2}}z^{-\frac{3}{2}}y^{\frac{1}{2}}}{(\tilde{A}_0-\ln y)\ln y}dy,\end{aligned}\tag{33}$$

where $\Delta_0=[b(\Theta_{\max}-\Theta_{\min})\hat{D}_{\mathrm{m}}]^{-1}$. By applying the change-in-variable technique and [16, Eq. (3.352.3)], we have

$$\begin{aligned}F_{\gamma_{\mathrm{U}}^{\mathrm{3D}}}^{\mathrm{I}}(z)=&\Delta_0D_{\max}^3[p_1(z\tilde{d}_{\min}^{-1})-p_1(\tilde{\theta}_{\min})]\\&-\Delta_0(\tilde{C}_0)^{\frac{3}{2}}z^{-\frac{3}{2}}[p_2(z\tilde{d}_{\min}^{-1})-p_2(\tilde{\theta}_{\min})].\end{aligned}\tag{34}$$

Similar to the derivation of (34), we can get

$$\begin{aligned}F_{\gamma_{\mathrm{U}}^{\mathrm{3D}}}^{\mathrm{II}}(z)=&\int_{\tilde{\theta}_{\min}}^{\tilde{\theta}_{\max}}\frac{\Delta_0\tilde{A}_0D_{\max}^3y^{-1}}{(\tilde{A}_0-\ln y)\ln y}dy\\&-\int_{\tilde{\theta}_{\min}}^{\tilde{\theta}_{\max}}\frac{\Delta_0\tilde{A}_0(\tilde{C}_0)^{\frac{3}{2}}z^{-\frac{3}{2}}y^{\frac{1}{2}}}{(\tilde{A}_0-\ln y)\ln y}dy\\=&\Delta_0D_{\max}^3[p_1(\tilde{\theta}_{\max})-p_1(\tilde{\theta}_{\min})]\\&-\Delta_0(\tilde{C}_0)^{\frac{3}{2}}z^{-\frac{3}{2}}[p_2(\tilde{\theta}_{\max})-p_2(\tilde{\theta}_{\min})],\end{aligned}\tag{35}$$

and

$$\begin{aligned}F_{\gamma_{\mathrm{U}}^{\mathrm{3D}}}^{\mathrm{III}}(z)=&1+\int_{\frac{z}{\tilde{d}_{\max}}}^{\tilde{\theta}_{\max}}\frac{\Delta_0\tilde{A}_0D_{\min}^3y^{-1}}{\left(\tilde{A}_0-\ln y\right)\ln y}dy\\&-\int_{\frac{z}{\tilde{d}_{\max}}}^{\tilde{\theta}_{\max}}\frac{\Delta_0\tilde{A}_0\left(\tilde{C}_0\right)^{\frac{3}{2}}z^{-\frac{3}{2}}y^{\frac{1}{2}}}{\left(\tilde{A}_0-\ln y\right)\ln y}dy\\=&1+\Delta_0D_{\min}^3[p_1(\tilde{\theta}_{\max})-p_1(z\tilde{d}_{\max}^{-1})]\\&-\Delta_0(\tilde{C}_0)^{\frac{3}{2}}z^{-\frac{3}{2}}[p_2(\tilde{\theta}_{\max})-p_2(z\tilde{d}_{\max}^{-1})].\end{aligned}\tag{36}$$

REFERENCES

[1] Y. Zeng, R. Zhang, and T. J. Lim, "Wireless communications with unmanned aerial vehicles: Opportunities and challenges," *IEEE Commun. Mag.*, vol. 54, no. 5, pp. 36–42, May 2016.
[2] X. Pang, M. Sheng, N. Zhao, J. Tang, D. Niyato, and K. -K. Wong, "When UAV meets IRS: Expanding air-ground networks via passive reflection," *IEEE Wireless Commun.*, vol. 28, no. 5, pp. 164–170, Oct. 2021.
[3] X. Yuan, Y. Hu, J. Zhang, and A. Schmeink, "Joint user scheduling and UAV trajectory design on completion time minimization for UAV-aided data collection," *IEEE Trans. Wireless Commun.*, to appear.
[4] N. Zhao *et al.*, "UAV-assisted emergency networks in disasters," *IEEE Wireless Commun.*, vol. 26, no. 1, pp. 45–51, Feb. 2019.
[5] Y. Polyanskiy, H. V. Poor, and S. Verdu, "Channel coding rate in the finite blocklength regime," *IEEE Trans. Inf. Theory*, vol. 56, no. 5, pp. 2307–2359, May 2010.
[6] H. Ren *et al.*, "Achievable data rate for URLLC-enabled UAV systems with 3-D channel model," *IEEE Wirel. Commun. Lett.*, vol. 8, no. 6, pp. 1587–1590, Dec. 2019.
[7] K. Wang *et al.*, "Packet error probability and effective throughput for ultra-reliable and low-latency UAV communications," *IEEE Trans. Commun.*, vol. 69, no. 1, pp. 73–84, Jan. 2021.
[8] S. Yan, S. V. Hanly, and I. B. Collings, "Optimal transmit power and flying location for UAV covert wireless communications," *IEEE J. Sel. Areas Commun.*, vol. 39, no. 11, pp. 3321–3333, Nov. 2021.
[9] X. Zhou, S. Yan, D. W. K. Ng, and R. Schober, "Three-dimensional placement and transmit power design for UAV covert communications," *IEEE Trans. Veh. Technol.*, vol. 70, no. 12, pp. 13 424–13 429, Dec. 2021.
[10] W. Yang *et al.*, "Wiretap channels: Nonasymptotic fundamental limits," *IEEE Trans. Inf. Theory*, vol. 65, no. 7, pp. 4069–4093, Jul. 2019.
[11] Y. Wang *et al.*, "UAV-enabled secure communication with finite block-length," *IEEE Trans. Veh. Tech.*, vol. 69, no. 12, pp. 16309–16313, Dec. 2020.
[12] Z. Ding *et al.*, "On the performance of non-orthogonal multiple access in 5G systems with randomly deployed users," *IEEE Signal Process. Lett.*, vol. 21, no. 12, pp. 1501–1505, Dec. 2014.
[13] W. Yi, Y. Liu, A. Nallanathan, and M. Elkashlan, "Clustered millimeter wave networks with non-orthogonal multiple access," *IEEE Trans. Commun.*, vol. 67, no. 6, pp. 4350–4364, Jun. 2019.
[14] Z. Wei, L. Yang, D. W. K. Ng, J. Yuan, and L. Hanzo, "On the performance gain of NOMA Over OMA in uplink communication systems," *IEEE Trans. Commun.*, vol. 68, no. 1, pp. 536–568, Jan. 2020.
[15] A. Al-Hourani *et al.*, "Optimal LAP altitude for maximum coverage," *IEEE Wireless Commun. Lett.*, vol. 3, no. 6, pp. 569–572, Dec. 2014.
[16] I. S. Gradshteyn and I. M. Ryzhik, *Table of Integrals, Series, and Products*, 7th ed. San Diego, CA, USA: Academic, 2007.
[17] Y. Xie and P. Ren, "Optimizing training and transmission overheads for secure URLLC against randomly distributed eavesdroppers," *IEEE Trans. Veh. Technol.*, vol. 71, no. 11, pp. 11921–11935, Nov. 2022.
[18] H. Wang, Q. Yang, Z. Ding, and H. V. Poor, "Secure short-packet communications for mission-critical IoT applications," *IEEE Trans. Wireless Commun.*, vol. 18, no. 5, pp. 2565–2578, May 2019.
[19] B. Makki, T. Svensson, and M. Zorzi, "Wireless energy and information transmission using feedback: Infinite and finite block-length analysis," *IEEE Trans. Commun.*, vol. 64, no. 12, pp. 5304–5318, Dec. 2016.
[20] N. Ari, N. Thomos and L. Musavian, "Performance analysis of short packet communications with multiple eavesdroppers," *IEEE Trans. Commun.*, vol. 70, no. 10, pp. 6778–6789, Oct. 2022.
[21] "Technical specification group radio access network; Study on enhanced LTE support for aerial vehicles (release 15)," 3GPP, Sophia Antipolis, France, TR 36.777, Dec. 2017.